Identification of Nonlinear Corrections to Multicopter Flight Simulation Model Using Machine Learning

Gaurav Makkar PhD Student
Robert Niemiec Research Scientist
Farhan Gandhi Redfern Chair, Director
Center for Mobility with Vertical Lift (MOVE)
Rensselaer Polytechnic Institute
Troy, NY United States

ABSTRACT

This study presents a novel methodology for identifying nonlinear corrections to improve the accuracy of a physics-based simulation model of a hexacopter using flight test data. Two distinct models are employed to capture the dynamics of the hexacopter in hover: one model is identified from flight data, and the other utilizes a physics-based blade element model with a 10-state Peter-He inflow. An input filter is extracted based on the difference between the flight test data and frequency response from the physics-based model to make corrections. This improves the predictions over the entire frequency range. For time domain analysis, the nonlinear corrections are identified by analyzing correlations between different flight variables and utilizing a filtered dataset with high normalized correlation. Regularized version of partial least squares is applied for identifying the correction terms. The performance of the updated linearized model is compared with the physics-based model and system ID model in the time domain for all four axes. It was observed that for low amplitude maneuvers, the performance of model with nonlinear corrections is comparable to the model identified from flight test data and sometimes slightly better (2-5%). Predictions obtained using the corrected model exhibit superior performance to those generated by the physics-based model, particularly in the vicinity of peak values (8%-14%). For large amplitude maneuvers, the distinction is even more pronounced, and the model with nonlinear corrections surpasses all other models in terms of accuracy. Notably, while the physics-based model predictions exhibit an average error of 32% when compared to the flight test data, and the model identified using flight test data generated predictions with an average error of 24%, the model with nonlinear corrections yielded predictions with an average error of less than 10%.

NOTATION

x	Vehicle x position
y	Vehicle y position
z	Vehicle z postion
ϕ	Roll attitude
θ	Pitch attitude
ψ	Heading
u	Longitudinal velocity
v	Lateral velocity
w	Heave velocity
p	Roll rate
q	Pitch rate
r	Yaw rate
δ_{thr}	Throttle control input
δ_{ele}	Longitudinal control input
δ_{ail}	Lateral control input
δ_{thr}	Yaw control input
δ_{u_M}	Mixer inputs for sweep
L_v	Speed damping - roll
L_p	Pitch damping
$L_{\delta_{lat}}$	Control derivative - Roll
M_u	Speed damping - pitch
M_q	Roll damping
$M_{\delta_{lon}}$	Control derivative - Pitch
N_r	Yaw damping
a_x	Linear correction coefficient
b_x	Cubic correction coefficient
λ	Regularization Factor

Presented at the Vertical Flight Society's 79th Annual Forum & Technology Display, West Palm Beach, FL, USA, May 16–18, 2023.

INTRODUCTION

Electric Vertical Takeoff and Landing (eVTOL) vehicles have seen massive technological advancement in recent years. The simple design of the drive systems and flexibility afforded by electric power distribution have lowered the barriers to entry for eVTOL design. Despite lower prototyping cost, flight simulation models of these eVTOL vehicles remain an invaluable tool for understanding these complex systems as they can be used for simulating new designs, configurations, operating conditions, or control strategies to explore their behavior.

A good simulation model reduces the need for costly experiments or field tests, but insights gained from these simulation models are contingent on the model being an accurate reflection of the underlying system. Accordingly, several groups

have developed means of correcting simulation models using flight test data to achieve the required fidelity (Refs. 1–5). The techniques of system identification provide a systematic framework for making corrections and enhancing a low-order physics-based simulation model derived from first principles and aircraft design data. It has been extensively used for fixed-wing aircraft (Refs. 6–8) and rotorcraft (Refs. 4, 9, 10).

The implementation of system identification techniques on conventional VTOL aircraft and their application on small-scale multicopters have been well documented in the literature. For instance, Wei and Ivler utilized the frequency domain system identification tool CIFER® (Ref. 11) to generate linear models of a quadcopter and hexacopter (Refs. 12, 13). Similarly, the U.S. Army Combat Capabilities Development Command Aviation and Missile Center conducted significant research on system identification and controller optimization for the IRIS+ quadcopter, with the aim of minimizing position response to turbulence inputs (Refs. 14, 15). These endeavors underscore the importance and potential benefits of employing advanced system identification methods.

NATO-AVT 296 summarizes the past several decades of technical work in the area of simulation fidelity improvement (Ref. 16). Model corrections can be identified in both the frequency domain (Refs. 17–22) and time domain (Refs. 23, 24). Methods such as gain/time delay corrections (Refs. 17–19) and black box input/output filter corrections (Refs. 20–22) are employed in the frequency domain and don't modify the baseline low-order model. Another popular fidelity improvement method is force/moment increment which uses a comparison of stability and control derivatives identified from flight tests and simulation model to derive increments/decrements that are added to the baseline model (Refs. 2, 5). The additive system identification approach for model fidelity improvement developed by Agarwal et. al (Ref. 23) applied to B-412 flight test data works in the time domain by identifying the derivatives in sequence depending on the dominant force/moment contribution to investigate the complex nonlinearities arising form aerodynamic couplings.

Reduced order models have been utilized to improve the baseline model by adding physics-based model structures for higher order effects such as inflow dynamics, and rotor-wake interference (Ref. 25). Model stitching has been combined with other methods to further improve the simulation results. In Ref. 26 the stitched model built from the identified 11-DOF model is improved by a black-box input filter method to account for unmodeled engine/drivetrain dynamics. Hui et al. (Ref. 27) also implemented reduced order models for updates at the edge-of-the-envelope maneuvers like takeoff, autorotation, and landing.

Most of these conventional system identification approaches process the complete time history, and therefore the identified derivatives represent an average for the whole maneuver. The force contribution to a rotorcraft motion should be identified when they are strongest during the maneuver (Ref. 23). Also, the corrections obtained by the frequency domain system identification methods mentioned above are linear in nature and thus only valid for "small-amplitude" maneuvers and disturbances. These methods may fail to make suitable adjustments for the nonlinear effects arising from large-amplitude maneuvers, which unmanned drones are capable of executing.

The objective of this study is to leverage machine learning techniques to identify nonlinear corrections to a physics-based model using flight test data. The flight test data is analysed to identify instances of high correlation between different flight variables. This filtered dataset is then used to accurately identify the required corrections to the existing model, thereby improving its accuracy and effectiveness.

METHODOLOGY AND ANALYSIS

Figure 1: MOVE Hexacopter

The platform used in this study is MOVE hexacopter (Fig. 1). It is based on Tarot 680 Pro frame and has Cube Orange flight controller (Ref. 28) installed onboard. Detailed specifications of the aircraft are provided in Table 1. Two modeling methods are used for the hexacopter: frequency domain system identification using CIFER® (Ref. 11), and the Rensselaer Multicopter Analysis Code (RMAC) (Ref. 29) which is a physics-based modeling method. These models are discussed in the following section.

Table 1: Specifications for Hexacopter

Aircraft	
Weight, with battery	2.5kg
Hub-to-Hub	680 mm
Motor Weight	93 gm
Kv Rating	380 RPM/V
Rotor diameter	330 mm
Rotor Weight (each)	15 gm
Rotor Pitch	4.8 in

Frequency-Domain System Identification

Frequency domain system identification is a process to extract flight-accurate state-space models of the vehicle via frequency responses. For the present study, frequency sweeps were performed about hover. The automated sweeps were injected at the control mixer (Fig. 2). The data is collected using system ID mode in Ardupilot. Inputs, u_M (δ_{lat}, δ_{lon}, δ_{yaw}, and δ_{thr}) are measured at the input to the mixer and measured outputs (y) include angular rates (p,q,r), angular attitudes (ϕ, θ, ψ), and accelerometer readings (a_x,a_y, a_z). The frequency responses of the multirotor vehicle are identified from the mixer input to the aircraft response, for example, p/δ_{lat}. The model's predictive ability can be tested by verifying the performance with flight doublets in the time domain (Ref. 11).

Identification of state-space models relative to the mixer inputs is performed by optimizing the parameters in the state-space model to best fit the identified frequency responses from flight data. Since the present multicopter configuration has decoupled vehicle dynamics in hover, two 2-DOF models (roll and pitch), and two 1-DOF models (heave and yaw), can be identified independently. The model structure for dynamics in the four axes is given in Eqs. 1-4. Included in Eqs. 1-4 are first-order filters representing the rotational dynamics of the rotors.

$$\begin{bmatrix} \dot{v} \\ \dot{p} \\ \dot{\phi} \\ \dot{T}_{lat} \end{bmatrix} = \begin{bmatrix} Y_v & 0 & g & 0 \\ L_v & L_p & 0 & L_{\delta_{lat}} \\ 0 & 1 & 0 & 0 \\ 0 & 0 & 0 & -\omega_{lag} \end{bmatrix} \begin{bmatrix} v \\ p \\ \phi \\ T_{lat} \end{bmatrix} + \begin{bmatrix} 0 \\ 0 \\ 0 \\ \omega_{lag} \end{bmatrix} \begin{bmatrix} \delta_{lat} \end{bmatrix} \quad (1)$$

$$\begin{bmatrix} \dot{u} \\ \dot{q} \\ \dot{\theta} \\ \dot{T}_{lon} \end{bmatrix} = \begin{bmatrix} X_u & 0 & -g & 0 \\ M_u & M_q & 0 & M_{\delta_{lon}} \\ 0 & 1 & 0 & 0 \\ 0 & 0 & 0 & -\omega_{lag} \end{bmatrix} \begin{bmatrix} u \\ q \\ \theta \\ T_{lon} \end{bmatrix} + \begin{bmatrix} 0 \\ 0 \\ 0 \\ \omega_{lag} \end{bmatrix} \begin{bmatrix} \delta_{lon} \end{bmatrix} \quad (2)$$

$$\begin{bmatrix} \dot{r} \\ \dot{T}_{yaw} \end{bmatrix} = \begin{bmatrix} N_r & N_{\delta_{yaw}} \\ 0 & -\omega_{lag} \end{bmatrix} \begin{bmatrix} r \\ T_{yaw} \end{bmatrix} + \begin{bmatrix} N_{\delta_{yaw}} \\ \omega_{lag} \end{bmatrix} \begin{bmatrix} \delta_{yaw} \end{bmatrix} \quad (3)$$

$$\begin{bmatrix} \dot{w} \\ \dot{T}_{thr} \end{bmatrix} = \begin{bmatrix} Z_w & Z_{\delta_{thr}} \\ 0 & -\omega_{lag} \end{bmatrix} \begin{bmatrix} w \\ T_{thr} \end{bmatrix} + \begin{bmatrix} 0 \\ \omega_{lag} \end{bmatrix} \begin{bmatrix} \delta_{thr} \end{bmatrix} \quad (4)$$

Rensselaer Multicopter Analysis Code

The Rensselaer Multicopter Analysis Code (RMAC) is a physics-based tool designed for the comprehensive analysis of multicopters. The vehicle is modeled as a 6-DOF, second-order dynamic rigid body. The equations of motion are rewritten in first-order form by introducing kinematic states for the position and attitude of the aircraft, whose derivatives are given by Eq. 5-6, where the 3x3 matrix R represents a rotation matrix that rotates a vector from the body-attached reference frame to the inertial reference frame, and matrix B expresses the rates of change of the 3-2-1 Euler angles in terms of the body angular velocities.

$$\begin{bmatrix} \dot{x} \\ \dot{y} \\ \dot{z} \end{bmatrix} = R \begin{bmatrix} u \\ v \\ w \end{bmatrix} = R\vec{V} \quad (5)$$

$$\begin{bmatrix} \dot{\phi} \\ \dot{\theta} \\ \dot{\psi} \end{bmatrix} = B \begin{bmatrix} p \\ q \\ r \end{bmatrix} = B\vec{\omega} \quad (6)$$

The linear and angular accelerations of the hexacopter can be evaluated through a simple summation of forces and moments about the center of gravity. The forces include gravity, drag, and rotor forces. Fuselage drag and rotor forces also induce moments about the center of gravity. Coriolis and inertial coupling effects are also included since the equilibrium equations are resolved in the non-inertial body-attached reference frame (Eq. 7 and 8).

$$\begin{bmatrix} \dot{u} \\ \dot{v} \\ \dot{w} \end{bmatrix} = R^T \begin{bmatrix} 0 \\ 0 \\ g \end{bmatrix} + \frac{1}{m}\left(D_{fuselage} + \sum_{i=1}^{6} F \right) - \vec{\omega} \times \vec{V} \quad (7)$$

$$\begin{bmatrix} \dot{p} \\ \dot{q} \\ \dot{r} \end{bmatrix} = I^{-1}\left(\vec{r_D} \times D_{fuselage} + \sum_{i=1}^{6} (M_i + \vec{r}_i \times \vec{F}_i) \right) \quad (8)$$

RMAC calculates the rotor forces and moments using blade element theory and a 10-state Peters-He dynamic inflow model (Ref. 30). The inflow dynamics take the form of Eq. 9

$$M\overset{*}{\alpha} + VL^{-1}\alpha = \frac{1}{2}\tau \quad (9)$$

The motors are modeled as DC motors with negligible inductance, with the dynamics taking the form of Eq. 10, and manufacturer-specified values for the motor parameters K_t (torque constant) and R_a (armature resistance). This model requires a throttled voltage input (V_i) to model the motor, so a conversion factor from the recorded PWM outputs is also identified prior to model comparison.

$$J\dot{\Omega}_i = \frac{K_t}{R_a}V_i - \frac{K_t^2}{R_a}\Omega_i - Q_i \quad (10)$$

Linear approximations to the dynamics can be generated by perturbing the aircraft states about a trim condition and estimating stability derivatives using a centered difference approximation. Similarly, control derivatives can be evaluated by perturbing the control inputs about the equilibrium condition. Both predictions of the inflow and motor dynamics are high-frequency (relative to the rigid body dynamics) and stable, and therefore the associated states are removed via static condensation, which results in a 12-state, 4-input-state space model (Eq. 11-14).

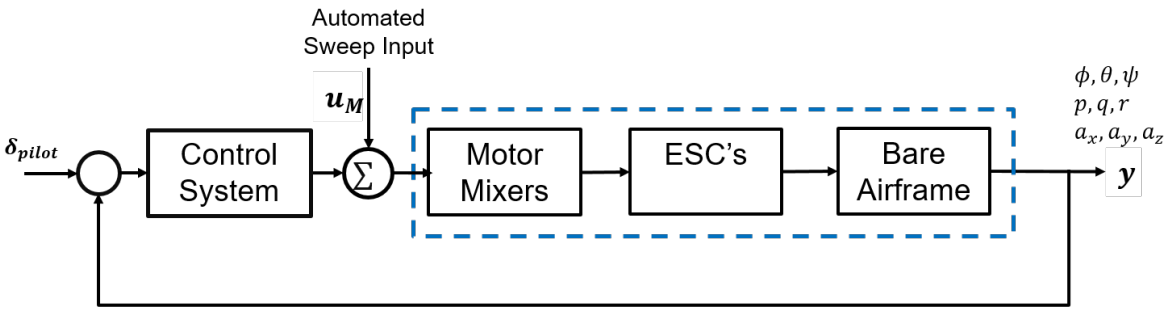

Figure 2: Block Diagram for System Identification Process using Flight test data

$$\begin{bmatrix} \dot{x_R} \\ \dot{x_I} \end{bmatrix} = \begin{bmatrix} A_{RR} & A_{RI} \\ A_{IR} & A_{II} \end{bmatrix} \begin{bmatrix} x_R \\ x_I \end{bmatrix} + \begin{bmatrix} B_R \\ B_I \end{bmatrix} u \tag{11}$$

$$\dot{x_R} = \bar{A} x_R + \bar{B} u \tag{12}$$

$$\bar{A} = A_{RR} - A_{RI} A_{II}^{-1} A_{IR} \tag{13}$$

$$\bar{B} = B_R - A_{RI} A_{II}^{-1} B_I \tag{14}$$

Methodology for Identifying Nonlinear Corrections

This section describes the proposed methodology for identifying nonlinear corrections. The corrections are applied to the physics-based linearized model of the hexacopter (low-fidelity model). For a linearized system, the roll acceleration is given by Eq. 15

$$\dot{p} = L_p p + L_v v + L_{\delta_{lat}} \delta_{lat} \tag{15}$$

where $\dot{p}$ is the roll acceleration, p is the roll rate, v represents lateral velocity, and δ_{lat} is the control input. The stability and control derivatives are assigned numerical values based on the linearized RMAC model. To model nonlinear dynamics, the above equation is updated with cubic terms in p and v. The updated roll acceleration is given in Eq. 16. The coefficients a_{L_p} and a_{L_v} represent corrections to the linear dynamics predicted by RMAC, while b_{L_p} and b_{L_v} represent nonlinear effects.

$$\begin{aligned} \dot{p} = & L_{p_{RMAC}} p (a_{L_p} + b_{L_p} p^2) + L_{v_{RMAC}} v (a_{L_v} + b_{L_v} v^2) \\ & + L_{\delta_{lat}} \delta_{lat} \end{aligned} \tag{16}$$

To identify numerical values for the a and b coefficients, 2480 seconds of flight test data are analyzed. A naive way of identifying these parameters would be to use all the data and fit a polynomial function that meets the required tolerance. Since the data is acquired from flight tests on different days with different conditions, disturbances including noise can lead to a poor fit if the model is not tuned appropriately. Also, the data at the start and end of a flight test is not particularly useful to predict the nonlinear behavior of the aircraft. With these in consideration, this study makes use of the correlation between different flight variables recorded during the flight tests to identify ideal data for identification.

Fig. 3 shows 40 seconds of roll acceleration ($\dot{p}$, Fig. 3a), roll rate (p, Fig. 3b), and lateral velocity data (v, Fig. 3c). This data is pared down based on the correlation between the roll acceleration and the roll rate or lateral velocity. To identify intervals of high correlation, the data is broken into one-second intervals (bins), and the correlation within each interval is evaluated, and the normalized correlation values are calculated (Figure 4). Bins where the absolute value of correlation between $\dot{p}$ and p exceeds 0.5 (represented by dotted black lines in Fig. 4) are used to identify corrections to L_p (a_{L_p} and b_{L_p}). Bin 22 highlighted in Fig. 4 represents one of the bins used for the exercise. Similarly, all the bins are examined and a filtered dataset with high correlation between $\dot{p}$ and p is extracted from the entire dataset. A similar process is used for identifying corrections to speed damping L_v (a_{L_v} and b_{L_v}).

These parameters are identified using a machine learning algorithm called Regularized Partial Least Squares (RPLS, Ref. 31, 32). RPLS is a modified version of Partial Least Squares (PLS) that includes a regularization penalty to prevent overfitting and improve the model's predictive performance. This is important since the data is noisy. The model is cross-validated to evaluate the performance of the model by splitting the data into training and validation sets multiple times and computing the average performance metric (RMSE) across all splits.

The optimization problem is given by

$$\min_{c,W} ||Y - XWc^T||^2 + \lambda (||W||^2 + ||c||^2) \tag{17}$$

where X is the predictor variable, Y is the response variable, and λ is the regularization parameter, W is the PLS weight matrix and c is the PLS weight vector and can be used to extract the coefficients a and b by the dot product of appropriate row of W with c (Refs. 32, 33). First, the data is normalized or scaled as necessary to ensure that variables with larger magnitudes do not dominate the analysis. The guidelines specified in Ref. 11 ($1ft = 1ft/s = 1deg = 1deg/s$) are used. The data is then split into training and testing sets. For this study, 80% data is used for training (and validating) and the remaining is reserved for testing. The hyperparameter in this study is the regularization parameter λ, which determines the shrinkage applied to the coefficients of the predictor variable. Once

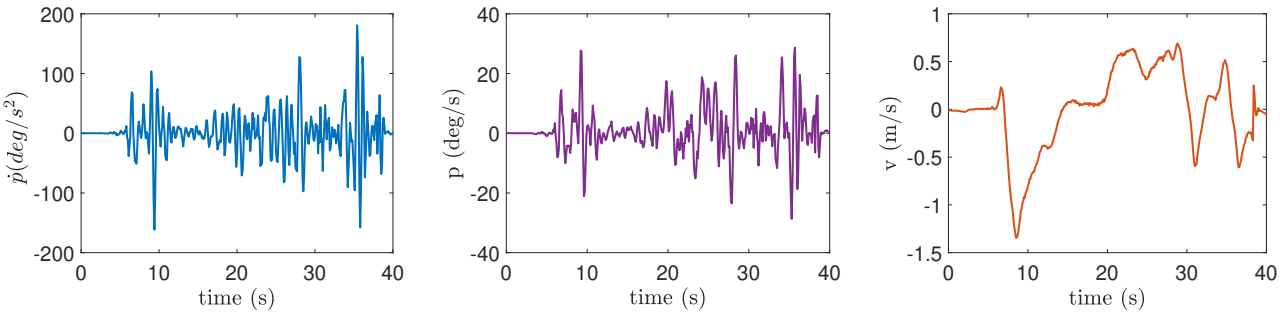

(a) $\dot{p}$ vs t (b) p vs t (c) v vs t

Figure 3: Flight test data

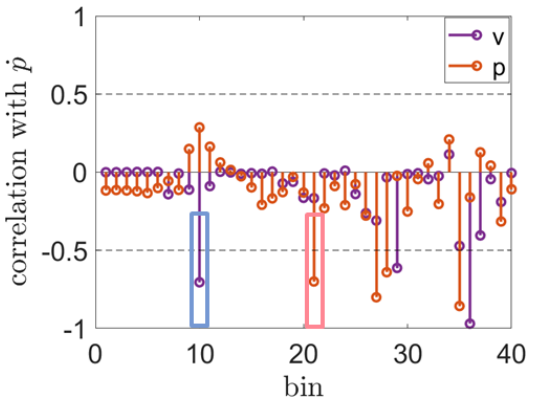

Figure 4: Correlation of p, and v with $\dot{p}$

the model is trained, the generalization characteristics of the trained model can be tested on the test set and the hyperparameter can be tuned.

The final equation for the roll rate ($\dot{p}$), lateral velocity (v), and roll (ϕ) after identifying the corrections is given in Eq. 18

$$\begin{aligned}\dot{p} =& L_{p_{RMAC}} p(0.03+0.6p^2) + L_{v_{RMAC}} v(0.65+0.62v^2) \\ &+ L_{\delta_{lat}} \delta_{lat} \\ \dot{v} =& Y_{v_{RMAC}} v(0.85+0.12v^2) - g\phi \\ \dot{\phi} =& p\end{aligned} \tag{18}$$

Similarly, the corrections for other axes can be identified. The updated equations are given in Eq. 19-21.

$$\begin{aligned}\dot{q} =& M_{q_{RMAC}} q(0.05+0.6q^2) + M_{u_{RMAC}} u(0.72+0.42u^2) \\ &+ L_{\delta_{lon}} \delta_{lon} \\ \dot{u} =& X_{u_{RMAC}} v(0.85+0.12v^2) - g\theta \\ \dot{\theta} =& q\end{aligned} \tag{19}$$

$$\dot{r} = N_{r_{RMAC}} r(0.18+0.1r^2) + N_{\delta_{yaw}} \delta_{yaw} \tag{20}$$

$$\dot{w} = Z_{w_{RMAC}} w(0.48+0.05w^2) + Z_{\delta_{thr}} \delta_{thr} \tag{21}$$

RESULTS

Frequency Domain

The fidelity of models derived through the systematic process of system identification, and using RMAC, is evaluated against flight test data in the frequency domain. The model structure outlined in Eq. 1-4 is used for both cases. For the system identification model, theoretical accuracy parameters, Cramér Rao (CR) bounds and insensitivity (I) are also reported (Ref. 11). These parameters carry substantial significance in the process of determining the model structure, owing to their role in eliminating the stability and control derivatives that exhibit weak theoretical accuracy/importance and are unidentifiable/irrelevant. It is desired that $CR < 20\%$, and $I < 10\%$. For the RMAC model, these parameters are not used since the parameters are directly identified using a perturbation method.

The resulting stability and control derivative values for both models are shown in Table 2. The parameters not shown in the table have zero values. It is important to note that the model was subjected to constraints to ensure the preservation of symmetry in the underlying physics. For example, the identified model was set up so that $X_u = Y_v$ and $L_v = -M_u$.

The verification of the models in the frequency domain is carried out qualitatively by overlaying the predictions from the models with the flight test data. Fig. 5 and 6 show the frequency response validation for roll attitude and roll rate from lateral input, respectively. The black solid line in these figures represents the flight test data. The orange dashed and yellow dashed lines represent the frequency response obtained using the model identified in CIFER® and the linearized RMAC model, respectively. The results clearly illustrate that the system identification model has an excellent fit and RMAC overpredicts the gain and phase across the frequency range. This occurs because the manufacturer-reported motor parameters result in motor dynamics that are significantly faster than those identified from the flight test data.

Based on the difference in gain and phase between the flight test and RMAC, a first-order error function can be identified. Fig. 7 shows the error between the model identified from the flight test and RMAC (plotted in solid blue) and its first-order

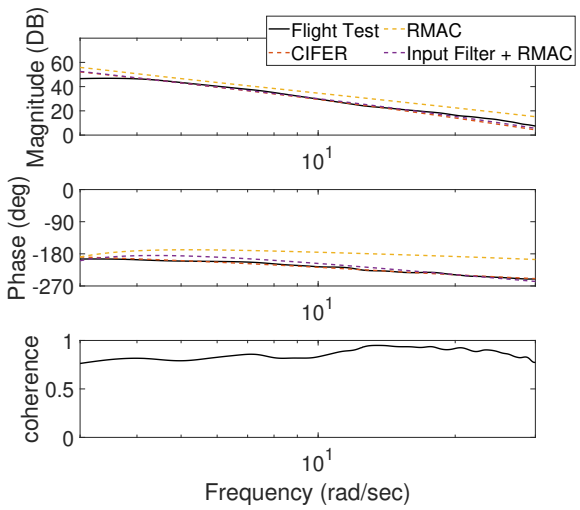

Figure 5: Hover Frequency Response: $\frac{\phi}{\delta_{ail}}$

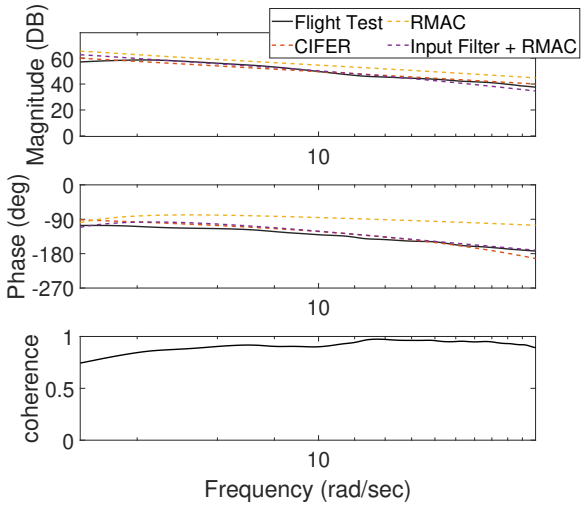

Figure 6: Hover Frequency Response : $\frac{p}{\delta_{ail}}$

Table 2: Stability and Control Derivatives

	CIFER			RMAC
	Value	**CR(%)**	**I(%)**	**Value**
Stability Derivatives				
$X_u(1/s)$	0	-	-	-0.05
$Y_v(1/s)$	0	-	-	-0.05
$Z_w(1/s)$	-0.22	19.8	9.4	-0.55
$L_v(rad/m-s)$	-1.67	6.32	2.42	-2.39
$L_p(1/s)$	0	-	-	-2.21
$M_u(rad/m-s)$	1.67	6.32	2.42	2.39
$M_q(1/s)$	0	-	-	-2.21
$M_w(rad/(m-s))$	0	-	-	0
$N_r(1/s)$	0	-	-	-0.17
$\omega_{lag}(rad/s)$	15.4	11.2	4.8	-
Control Derivatives				
$Z_{\delta_{thr}}\left(\frac{m/s^2}{\%/100}\right)$	-35	3.35	2.14	-42.2
$L_{\delta_{lat}}\left(\frac{rad/s^2}{\%/100}\right)$	58.6	3.38	1.98	36.2
$M_{\delta_{lon}}\left(\frac{rad/s^2}{\%/100}\right)$	58.6	3.84	1.78	36.2
$N_{\delta_{yaw}}\left(\frac{rad/s^2}{\%/100}\right)$	38.4	5.42	1.22	26.7

approximation (plotted in solid red). The first-order function approximates the error well. This error function evaluated for the roll axis is given in Eq. 22. This error function can be used as an input filter for correction by placing it upstream of the baseline model (Figure 8). The updated frequency response, for roll and roll rate with the input filter, is represented by the purple dashed line in Fig. 5 and 6. The predictions after including the input filter move the curve closer to the CIFER®identified model.

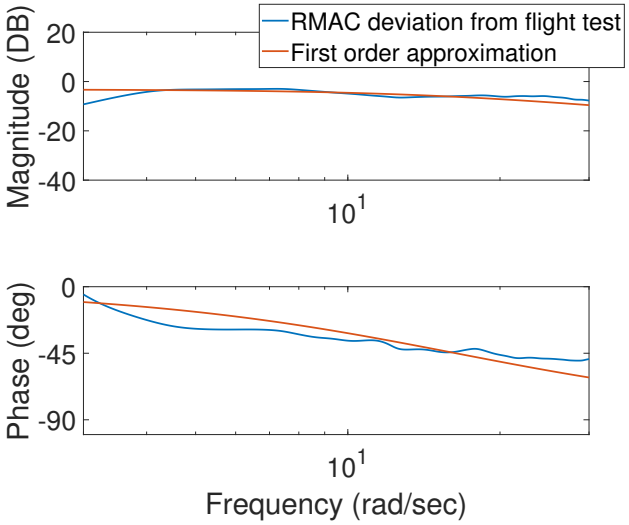

Figure 7: First order approximation of the difference between model identified from flight test, and RMAC

$$E_{Roll} = 0.71\frac{15.5}{s+15.5} \tag{22}$$

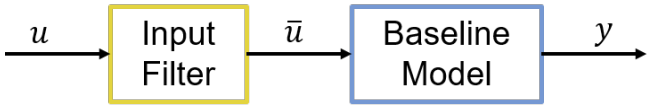

Figure 8: Input Filter

Similarly, for pitch attitude and pitch rate, the frequency response is presented in Fig. 9 and Fig. 10 respectively. The behavior is similar to the roll axis, which is expected because

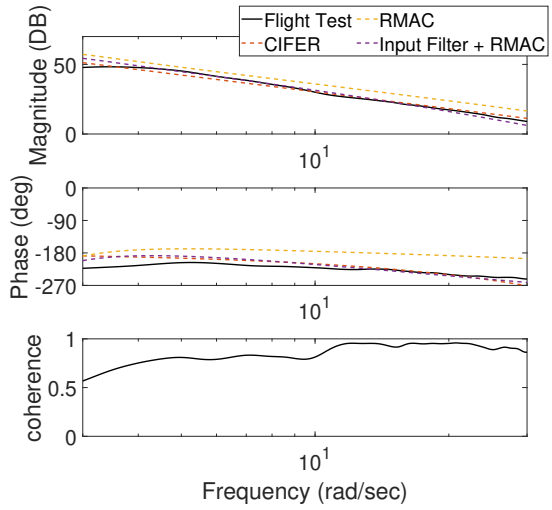

Figure 9: Hover Frequency Response: $\frac{\theta}{\delta_{ele}}$

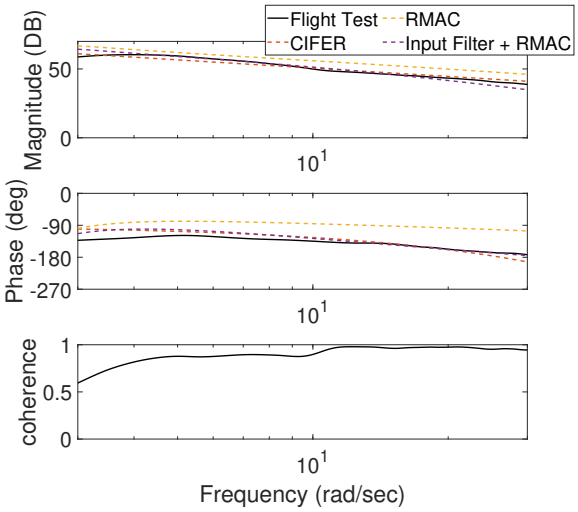

Figure 10: Hover Frequency Response : $\frac{q}{\delta_{ele}}$

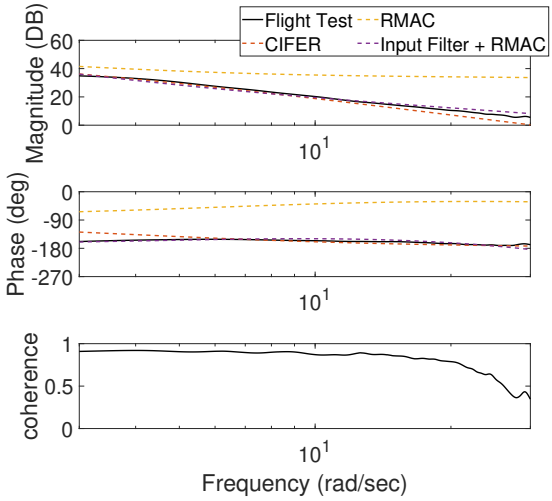

Figure 11: Hover Frequency Response: $\frac{r}{\delta_{rud}}$

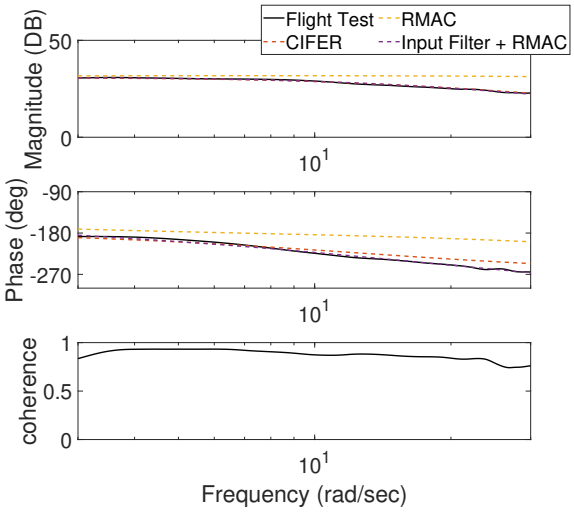

Figure 12: Hover Frequency Response : $\frac{a_z}{\delta_{thr}}$

of the symmetry of the aircraft. The frequency response for yaw and heave are shown in Fig. 11 and 12 respectively. Upon implementing the input filter corrections, the model demonstrated a notable improvement in accuracy across the entire frequency spectrum.

Next, to quantify the performance of these models, they can be compared using a cost function. The cost function is calculated by a weighted sum of time and frequency domain errors given by Eq. 23 (Ref. 11).

$$J_t = \frac{20}{n_\omega}\sum_{\omega_1}^{\omega_n} W_\gamma[W_g(|\hat{T}_c(\omega)| - |T(\omega)|)^2 + W_p(\angle\hat{T}_c(\omega) - \angle T(\omega))^2] \tag{23}$$

where $|T|,\angle T$ are the flight frequency response gain (dB) and phase (deg), $|\hat{T}_c|,\angle\hat{T}_c$ are the model frequency response gain and phase. Magnitude and phase error weightings are $W_g = 1$, and $W_p = 0.01745$. The coherence (γ) weighting employed in the cost function prioritizes the most precise (highest coherence) data by assigning them greater weightage. The cost can be calculated for each of the frequency responses that are included in the parametric model identification. A cost of $J_i < 100$ indicates an accurate model for that response and a cost of $J_i < 50$ is considered indistinguishable from the true model.

Table 3 compares the cost of fits obtained using different models. The cost of the system ID model is excellent for all responses, which is expected since the model was identified directly from flight test data. The costs associated with RMAC are significantly higher (> 100). When the simulation model is updated with an input filter, there is a substantial reduction in cost (85%-90%) and the cost is comparable to the model

identified from flight test data.

Table 3: Frequency Domain Verification Costs for System ID, RMAC and Corrected Models

	CIFER	RMAC	RMAC + Input Filter
$\frac{\phi}{\delta_{ail}}$	42.6	482	46.6
$\frac{p}{\delta_{ail}}$	52.1	416	62.4
$\frac{\theta}{\delta_{ele}}$	62.4	476	68.2
$\frac{q}{\delta_{ele}}$	56.4	482	58.6
$\frac{r}{\delta_{rudd}}$	48.2	568	58.2
$\frac{a_z}{\delta_{thr}}$	44.4	520	62.8

Time Domain

The verification of system identification models in the time domain constitutes a crucial final step in the validation process of models developed in the frequency domain. It is essential to test the robustness of the model against a different dataset and input signal to ensure that it is not excessively tuned to the data utilized to derive the frequency responses. Robustness to input variation is a fundamental indication that the model accurately represents the underlying physical processes and is not merely a generic curve fit of the data. When nonlinear corrections are applied, time domain verification is particularly significant, as it provides valuable insights into the predictive ability of a model that cannot be represented in the frequency domain.

First, consider the verification in the roll axis using different modeling methods in the time domain. The results are shown in Fig. 13, where Fig. 13a depicts the roll input, Fig. 13b shows the roll attitude, and 13d displays the roll rate. The flight test data is represented by the black solid line, while the predictions using the CIFER®-identified model is shown by the orange dashed line. These predictions are nearly indistinguishable from the flight test data. In contrast, the predictions from the RMAC model (yellow dashed) exhibit some magnitude overshoot relative to the flight test data.

Next, the performance of RMAC model with an input filter (Fig. 8) is evaluated. The results are shown in the purple dashed line in Fig. 13b and 13d. This approach yielded better performance in the frequency response plots (Fig. 5-9) as well. Additionally, predictions after applying nonlinear corrections evaluated using Eq. 18, are presented by the green-dashed line in Fig. 13b and 13d. The exhibited predictions are excellent and outperform both the CIFER®-identified model and the RMAC model updated with input filter near peaks.

These results are also reflected in the error plots for roll (Fig. 13c) and roll rate (Fig. 13e), where the error for the model identified from the flight test data (orange dashed) and the model corrected using identified derivatives (plotted in green dashed) is close to zero for the entire duration. In contrast, the error using the RMAC model (yellow dashed) reaches 6° around 1 second. However, this error is significantly reduced when an input filter is used to make corrections (plotted in purple dashed). The verification of the roll axis using different modeling methods in the time domain demonstrates that identified corrections can improve the accuracy of aircraft models to perform as well as the model identified from flight test data.

Similar verification exercises are carried out for the pitch (Fig. 14), yaw (Fig. 15), and heave axes (Fig. 16) using the same modeling methods in the time domain. The results show that identified corrections can improve the accuracy of aircraft models for these axes as well. The CIFER® model and models with nonlinear corrections produce predictions that closely match the flight test data, while the RMAC model exhibits overshoot in most cases. The input filter also proves to be an effective tool in improving the performance of the RMAC model for these axes. The models corrected with identified nonlinear corrections produce predictions that are comparable to or better than the CIFER®-identified model, demonstrating the importance of identified corrections in enhancing the accuracy of aircraft models in the time domain.

To quantitatively compare the performance, the time domain verification cost (Eq. 24) is evaluated.

$$J_{rms} = \sqrt{\frac{1}{n_t n_o}\sum_{i=1}^{n_t}(y_{data}-y)^T W (y_{data}-y)} \tag{24}$$

where y_{data} is the time-history vector from the flight data, y is the model time-history vector, n_t is the number of time-history points in the data record, and $W = n_o \times n_o$ is a diagonal matrix of weighting factors for each output. Ref. 11 has established the desired time domain cost for full-scale vehicles, which has been thoroughly examined. According to Ref. 11, achieving a predictive accuracy of $J_{rms} < 1$ is deemed excellent, while a range of $1 < J_{rms} < 2$ is considered acceptable. To determine the scaled costs for a smaller vehicle relative to the UH-60 Froude scaling was employed $\left(N = \frac{D_{hub-to-hub}}{D_{UH-60}} = 24.5\right)$. If the scaling is included, $J_{rms} < 4.95$ would indicate excellent predictions, and a range of $4.95 < J_{rms} < 9.90$ would be considered acceptable.

A normalized cost function, known as Theil inequality coefficient(TIC) (Eq. 25), is also evaluated for all models since it does not need to be scaled with vehicle size (Ref. 11). J_{rms} and TIC are summarized in Table 4 for all the axes.

$$TIC = \frac{J_{rms}}{\sqrt{\frac{1}{n_t n_o}\sum_{i=1}^{n_t}(y)^T W (y)} + \sqrt{\frac{1}{n_t n_o}\sum_{i=1}^{n_t}(y_{data})^T W (y_{data})}} \tag{25}$$

The results indicate that the system ID model has excellent predictive accuracy with J_{rms} and TIC well within guidelines. With the input filter applied, the RMAC model has excellent

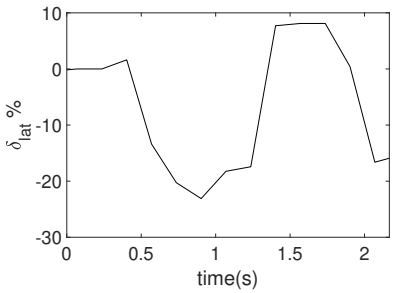

(a) Roll Input

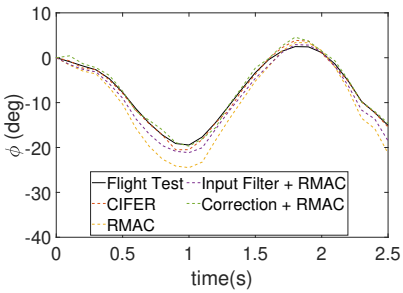

(b) Time domain validation: ϕ

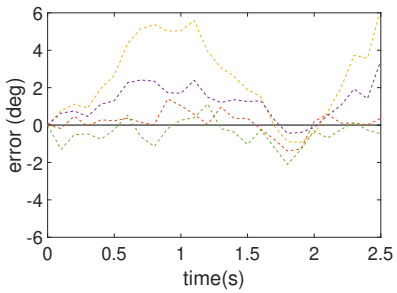

(c) Error from all models: ϕ

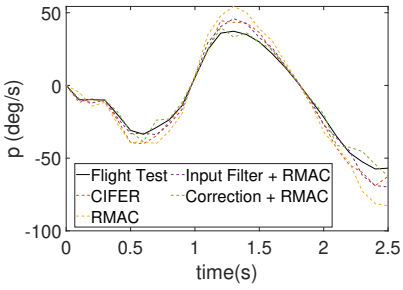

(d) Time domain validation: p

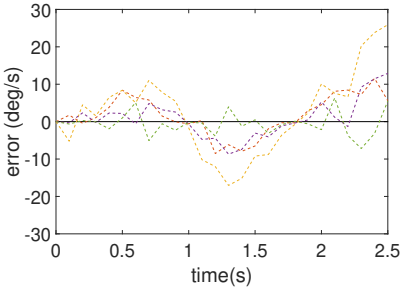

(e) Error from all models: p

Figure 13: Time domain validation: Roll axis

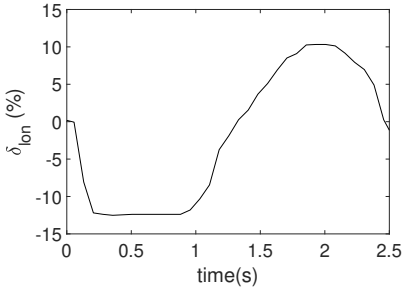

(a) Pitch Input

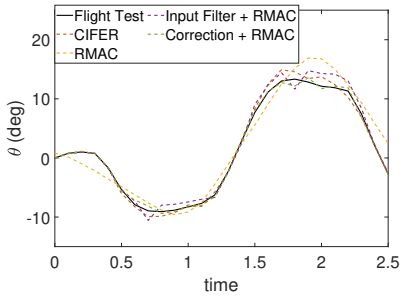

(b) Time domain validation: θ

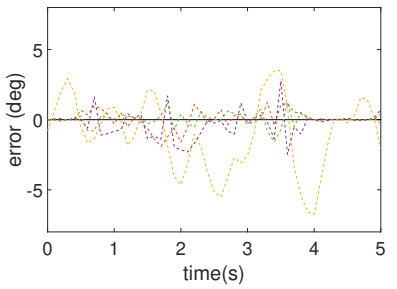

(c) Error from all models: θ

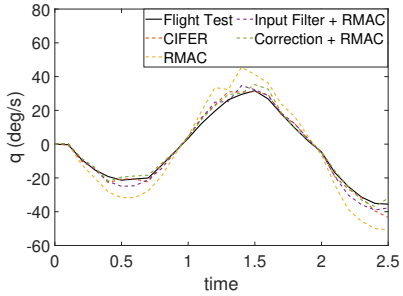

(d) Time domain validation: q

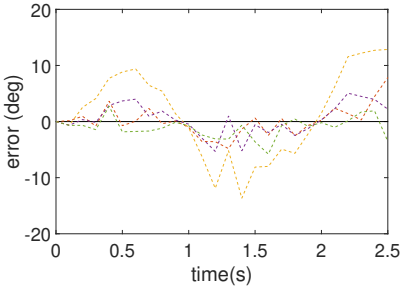

(e) Error from all models: q

Figure 14: Time domain validation: Pitch axis

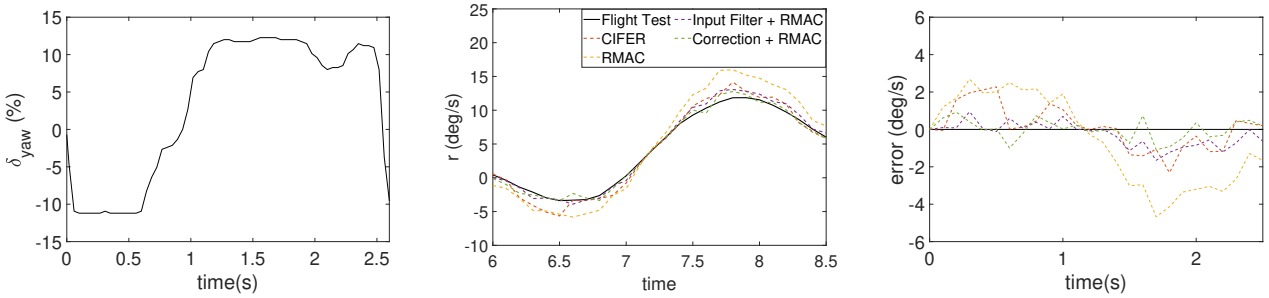

(a) Yaw Input (b) Time domain validation: r (c) Error from all models: r

Figure 15: Time domain validation: Yaw axis

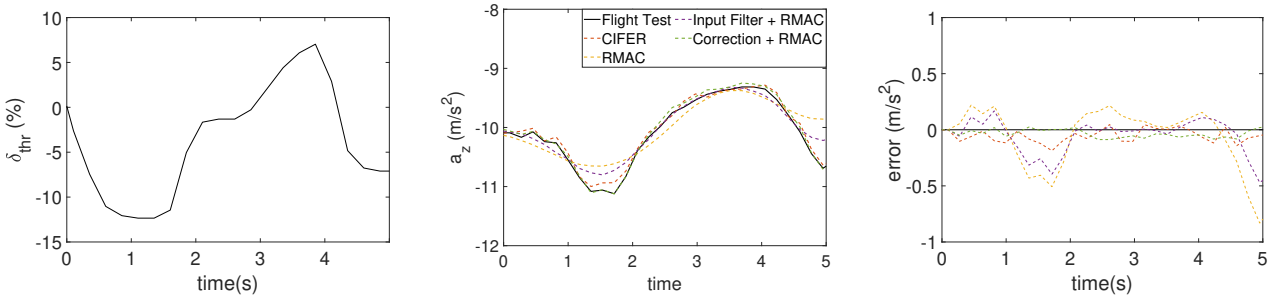

(a) Heave Input (b) Time domain validation: a_z (c) Error from all models: a_z

Figure 16: Time domain validation: Heave axis

Table 4: Time Domain Verification Costs for System ID, RMAC and Corrected Models - Low Amplitude

	Roll		**Pitch**		**Yaw**		**Heave**	
	J_{rms}	$TIC \times 100$	J_{rms}	$TIC \times 100$	J_{rms}	$TIC \times 100$	J_{rms}	$TIC \times 100$
CIFER	2.24	6.54	2.40	7.8	2.12	5.4	1.5	22.4
RMAC	7.54	18.6	7.82	19.2	8.12	19.6	7.25	31.2
RMAC + Input Filter	3.26	8.54	3.46	8.62	2.20	7.58	2.12	24.6
RMAC + Corrections	2.20	4.65	2.20	5.24	1.46	3.24	1.24	18.2

predictive accuracy, and the nonlinear corrections are comparable or superior to the CIFER®-identified model. Applying input filter corrections also lowers the TIC by more than 50% from the RMAC model for the roll, pitch, and yaw axis. The predictions are almost 70% - 84% more accurate with CIFER®-identified model and model with non-linear corrections.

Time Domain Verification - High Amplitude

With the performance of different models established for low-amplitude maneuvers, the next step is to examine the potential of corrected models with large-amplitude maneuvers, which are expected to have nonlinear effects. Since CIFER®-produced models are necessarily linear, they cannot include any nonlinear effects. Thus, it is expected that the RMAC model with nonlinear corrections will generally outperform the CIFER® model.

First, consider the roll axis predictions. The models' predictions are overlaid with flight test data to evaluate their accuracy in Fig. 17 for a high amplitude maneuver. The maximum roll attitude that the aircraft achieves is 41° (at 1 second). The predictions for roll (Fig. 17b) and roll rate (Fig. 17d) using all models are accurate during the start of the maneuver, as seen by the close grouping of CIFER®-identified (plotted in dashed orange), RMAC (plotted in dashed yellow), model corrected using input filter (plotted in dashed purple), and nonlinear corrections (plotted in dashed green) curves. However, these curves start to separate as the roll attitude reaches its maximum amplitude (around 1 second).

The aircraft maintains a steady roll attitude of 37° till 3 seconds before the attitude starts to drop again. The predictions using CIFER®-identified model have almost a steady error of 6° as shown by the orange dashed line in Fig. 17c. The analysis reveals that the predictions generated by the physics-based RMAC model exhibit a fluctuating error of around 10° during the high-amplitude aircraft maneuver (Fig. 17c, plotted in dashed yellow). Such unpredictability in the model's predictions could significantly impact the reliability and safety of autonomous systems that rely on these predictions. The error comes down to 6° when an input filter is used with the RMAC model (plotted in dashed purple). Finally, the predictions generated by the nonlinear corrections (Eq. 18) are found to be highly accurate, with an error of just 1° for most of the maneuver duration (Fig. 17c, plotted in dashed green).

The results of the analysis for pitch (Fig. 18), yaw (Fig. 19), and heave axis (Fig. 20) corroborate those obtained for the roll axis, indicating that the trends and observations were consistent across all axes. The accuracy of the models' predictions at the start of the maneuver, followed by the reduction in accuracy as the aircraft approached its maximum amplitude, is a common trend observed in all axes.

However, the inclusion of nonlinear corrections is found to be crucial for improving the accuracy of model predictions across all axes. The analyses demonstrate that the models' predictions achieve minimal errors when nonlinear corrections are incorporated, highlighting the importance of considering nonlinear effects in model development for all axes.

Overall, the results of the analysis indicate that the models' predictions outperform the CIFER®-identified model for all axes. These findings have significant implications for the development of autonomous systems, as accurate and reliable predictions of aircraft behavior are critical to ensuring the safety and efficiency of such systems.

The J_{rms} and TIC values for all the entire test dataset using different modeling methods are shown in Table 5. The analysis reveals that the RMAC model exhibits a larger error in predicting the aircraft's behavior compared to the other models resulting in higher J_{rms} and TIC values for the RMAC model, which fail to meet the guidelines set for acceptable predictive accuracy.

The model corrected using nonlinear corrections exhibits the highest predictive accuracy with J_{rms} and TIC values well within the guidelines. The incorporation of nonlinear corrections enables the model to capture the nonlinearities in the aircraft's behavior more accurately, leading to better predictive performance. The performance is better than the predictions from the CIFER®-model (29% - 62%). Furthermore, the implementation of the input filter results in a significant reduction in Jrms (40% - 62%) compared to RMAC, indicating an improvement in predictive accuracy.

The findings highlight the importance of incorporating nonlinear corrections to improve the predictive accuracy of autonomous systems, particularly in high-amplitude maneuvers.

CONCLUSIONS

This study examines a method for identifying nonlinear corrections to a physics-based multicopter flight simulation model using flight test data. A model is identified from the flight test data for comparing the performance of the corrected models. Based on the physics-based model and identified response from flight test data, an input filter is extracted, which is utilized to make linear corrections to the physics-based model in both the frequency and time domains.

To improve the predictions for high-amplitude maneuvers where the linear models provide inaccurate predictions, the stability derivatives for all four axes are supplemented with corrections in linear terms and additional cubic terms. To identify the nonlinear corrections to the physics-based model, the flight test data is examined to find regions with high correlations between different flight variables. Regularized Partial Least Squares is employed to ensure that the model is robust to noise and generalizes well.

In the frequency domain, the addition of an input filter improves the prediction across the frequency range and brings the RMAC model close to the CIFER® model. The predictions after applying corrections are excellent, especially in the high-frequency range critical to control design.

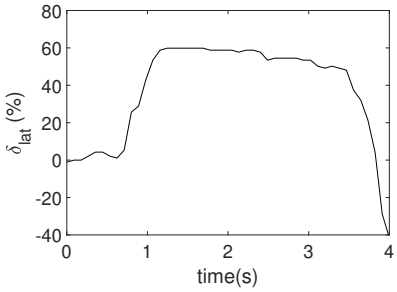

(a) Roll Input

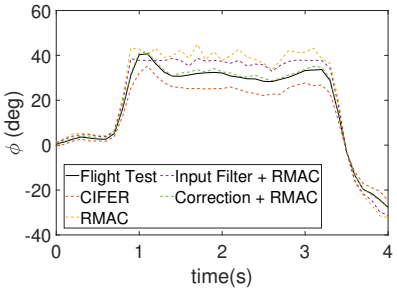

(b) Time domain validation: ϕ

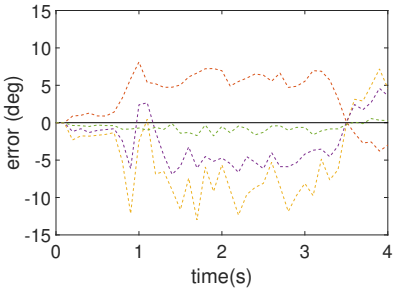

(c) Error from all models: ϕ

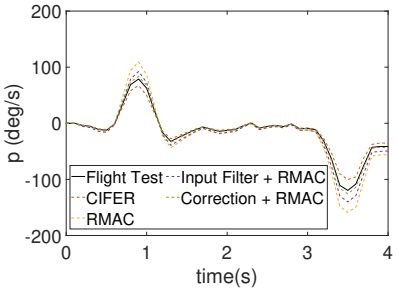

(d) Time domain validation: p

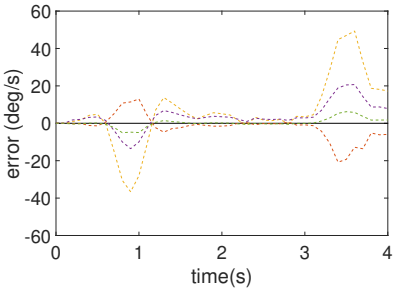

(e) Error from all models: p

Figure 17: Time domain validation - High Amplitude: Roll axis

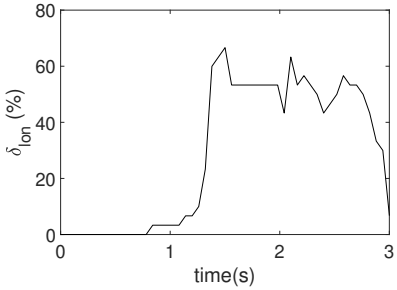

(a) Pitch Input

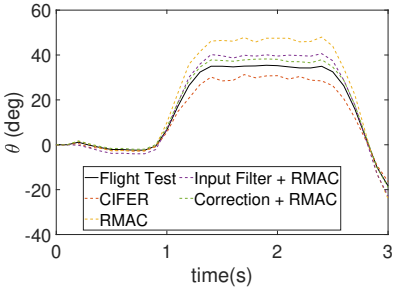

(b) Time domain validation: θ

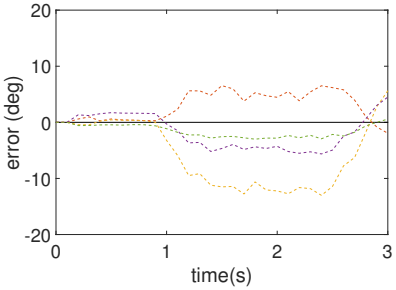

(c) Error from all models: θ

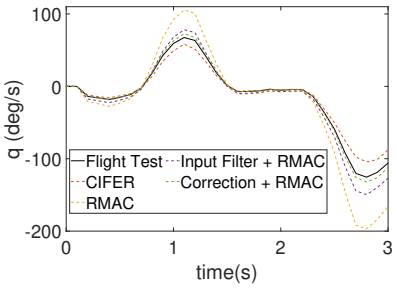

(d) Time domain validation: q

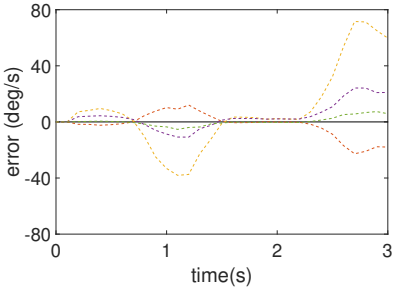

(e) Error from all models: q

Figure 18: Time domain validation - High Amplitude: Pitch axis

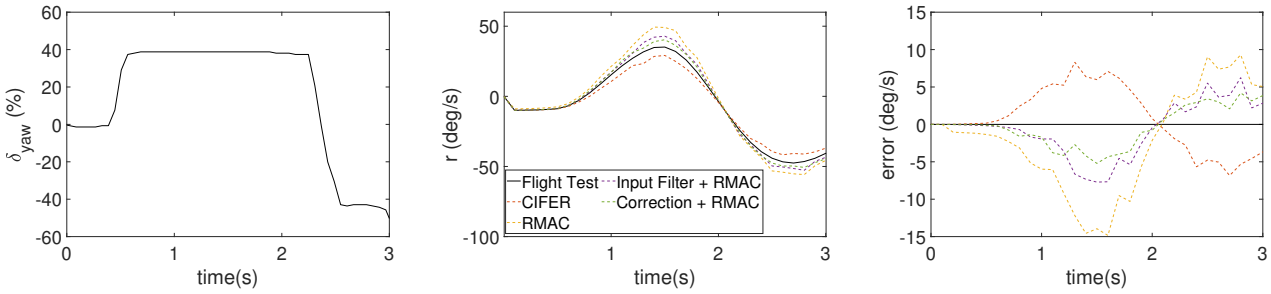

(a) Yaw Input (b) Time domain validation: r (c) Error from all models: r

Figure 19: Time domain validation - High Amplitude: Yaw axis

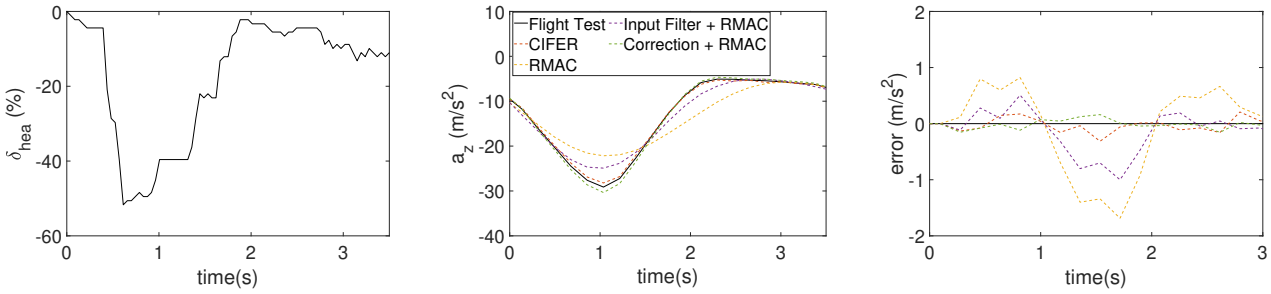

(a) Heave Input (b) Time domain validation: a_z (c) Error from all models: a_z

Figure 20: Time domain validation - High Amplitude: Heave axis

Table 5: Time Domain Verification Costs for System ID, RMAC, and Corrected Models - High Amplitude

	Roll		**Pitch**		**Yaw**		**Heave**	
	J_{rms}	$TIC \times 100$	J_{rms}	$TIC \times 100$	J_{rms}	$TIC \times 100$	J_{rms}	$TIC \times 100$
CIFER	10.9	24.4	11.8	22.4	9.5	17.4	2.24	30.4
RMAC	18.4	36.8	18.6	37.4	14.5	27.6	4.62	39.4
RMAC + Input Filter	11.2	27.6	12.4	27.4	10.7	22.0	2.64	32.6
RMAC + Corrections	6.64	9.80	6.36	10.2	5.24	12.2	1.98	30.0

To further validate the model corrections, low- and high-amplitude maneuvers were executed. For low amplitude maneuvers, the performance of the linearly corrected model is comparable to the identified model, exhibiting superior performance to predictions from the physics-based model, especially in the vicinity of peak values reducing the average error by 14%. Additionally, when predictions are generated using the model corrected with nonlinear corrections, the error reduces by 10% - 24% in comparison to the physics-based model. This model with identified corrections performs 2% - 5% better than the model identified from the flight test data.

For high-amplitude maneuvers, the distinction is even more pronounced. Notably, the model with nonlinear corrections surpasses all other methods in terms of accuracy. While the physics-based model predictions exhibit an average error of 32% when compared to the flight test data, and the model identified using flight test data generated predictions with an average error of 24%, the model with nonlinear corrections yields predictions with an average error of less than 10% for roll, pitch, and yaw axis. The performance in the heave axis is 24% better than the physics-based model. These results highlight the potential of utilizing nonlinear corrections to enhance the accuracy of multicopter flight simulation models.

REFERENCES

1. Fegely, C., Juhasz, O., Xin, H., and Tischler, M. B., "Flight dynamics and control modeling with system identification validation of the Sikorsky X2 Technology™ Demonstrator," American Helicopter Society 72nd Annual Forum, West Palm Beach, FL, 2016.

2. Seher-Weiß, S., Greiser, S., Wartmann, J., Myrand-Lapierre, V., Gubbels, A., Ricciardi, J., and Hui, K., "Bell 412 System Identification: Comparing Methods and Tools," *Vertical Flight Society 75th Annual Proceedings*, 2019.

3. Morelli, E. A., and Cooper, J., "Frequency-domain method for automated simulation updates based on flight data," *Journal of Aircraft*, Vol. 52, (6), 2015, pp. 1995–2008.

4. Cameron, N., White, M. D., Padfield, G. D., Lu, L., Agarwal, D., and Gubbels, A. W., "Rotorcraft modeling renovation for improved fidelity," Vertical Flight Society 75th Annual Forum, 2019.

5. Lu, L., Padfield, G., White, M., and Perfect, P., "Fidelity enhancement of a rotorcraft simulation model through system identification," *The Aeronautical Journal*, Vol. 115, (1170), 2011, pp. 453–470.

6. Drobik, J. S., and Brian, G. J., "Application of system identification techniques to the F-111C and PC 9/A aircraft," *Journal of aircraft*, Vol. 41, (4), 2004, pp. 744–751.

7. Morelli, E. A., and Klein, V., "Application of system identification to aircraft at NASA Langley Research Center," *Journal of Aircraft*, Vol. 42, (1), 2005, pp. 12–25.

8. Klein, V., and Morelli, E., "Aircraft system identification: theory and practice, American Institute of Aeronautics and Astronautics," *Inc., Reston, VA*, 2006.

9. Padfield, G., Thorne, R., Murray-Smith, D., Black, C., and Caldwell, A., "UK research into system identification for helicopter flight mechanics," *Vertica*, Vol. 11, (4), 1987, pp. 665–684.

10. Vitale, A., Genito, N., Federico, L., and Corraro, F., "Hybrid Approach for Rotorcraft Identification from Flight Data," American Helicopter Society, 67th Annual Forum, Virginia Beach, VA, 2011.

11. Tischler, M. B., and Remple, R. K., *Aircraft and rotorcraft system identification*, American Institute of Aeronautics and Astronautics Reston, VA, 2012.

12. Ivler, C., Niemiec, R., Gandhi, F., and Sanders, F. C., "Multirotor electric aerial vehicle model validation with flight data: Physics-based and system identification models," Vertical Flight Society 75th Annual Forum, Philidelphia, PA, USA, 2019.

13. Ivler, C. M., and Tischler, M. B., "Case studies of system identification modeling for flight control design," *Journal of the American Helicopter Society*, Vol. 58, (1), 2013, pp. 1–16.

14. Wei, W., Tischler, M. B., and Cohen, K., "System identification and controller optimization of a quadrotor unmanned aerial vehicle in hover," *Journal of the American Helicopter Society*, Vol. 62, (4), 2017, pp. 1–9.

15. Cheung, K. K., Wagster IV, J. A., Tischler, M. B., Ivler, C. M., Berrios, M. G., Berger, T., and Lehmann, R. M., "An overview of the US Army Aviation Development Directorate quadrotor guidance, navigation, and control project," Vertical Flight Society Forum, Vol. 73, 2017.

16. Tischler, M., and White, M., "Rotorcraft Flight Simulation Model Fidelity Improvement and Assessment-Final report of NATO STO AVT-296 Research Task Group," , 2021.

17. Kaplita, T., Driscoll, J., Difler, M., and Hong, S., "Helicopter simulation development by correlation with frequency sweep flight test data," AHS, Annual Forum, 45 th, Boston, MA, 1989.

18. Kaletka, J., and GRUENHAGEN, V., "Identification of mathematical derivative models for the design of a model following control system[(for fly-by-wire helicopter)]," *Vertica*, Vol. 13, (3), 1989, pp. 213–228.

19. Kaletka, J., Tischler, M. B., Fletcher, J. W., *et al.*, "Time and Frequency-Domain Identification and Verification of BO 105 Dynamic Models," *Journal of the American Helicopter Society*, Vol. 36, (4), 1991, pp. 25–38.

20. Greiser, S., "High-fidelity rotorcraft simulation model: analyzing and improving linear operating point models," *CEAS Aeronautical Journal*, Vol. 10, (3), 2019, pp. 687–702.

21. Šćepanović, P., and Döring, F. A., "Improving a real-time helicopter simulator model with linear input filters," *CEAS Aeronautical Journal*, Vol. 12, (3), 2021, pp. 605–619.

22. Miller, D. G., and White, F., "A treatment of the impact of rotor-fuselage coupling on helicopter handling qualities," AHS, Annual Forum, 43 rd, Saint Louis, MO, Proceedings., Vol. 2, 1987.

23. Agarwal, D., Lu, L., Padfield, G. D., Cameron, N., White, M. D., and Gubbels, A., "Rotorcraft Simulation Fidelity for Low Speed Manoeuvring Using 'Additive'System Identification," 45th European Rotorcraft Forum, 2019.

24. Chowdhary, G., Yucelen, T., Mühlegg, M., and Johnson, E. N., "Concurrent learning adaptive control of linear systems with exponentially convergent bounds," *International Journal of Adaptive Control and Signal Processing*, Vol. 27, (4), 2013, pp. 280–301.

25. Arnold, U. T., Keller, J. D., Curtiss, H., Reichert, G., *et al.*, "The effect of inflow models on the predicted response of helicopters," *Journal of the American Helicopter Society*, Vol. 43, (1), 1998, pp. 25–36.

26. Seher-Weiss, S., and von Grünhagen, W., "EC135 system identification for model following control and turbulence modeling," Paper CEAS-2007-275, Proccedings of the 1st CEAS European Air and Space Conference 2007, 2007.

27. Hui, K., Lambert, E., and Seto, J., "Bell M427 Flight Test Data Gathering and Level-D Simulator Model Development," , 2006.

28. "PX4 User Guide," https://docs.px4.io/main/en/flight_controller/cubepilot_cube_orange.html, [Online; accessed 17 October 2022].

29. Niemiec, R., and Gandhi, F., "Development and validation of the rensselaer multicopter analysis code (RMAC): a physics-based comprehensive modeling tool," 75th Annual Forum of the Vertical Flight Society, Philadelphia, PA, 2019.

30. Peters, D. A., Boyd, D. D., and He, C. J., "Finite-state induced-flow model for rotors in hover and forward flight," *Journal of the American Helicopter Society*, Vol. 34, (4), 1989, pp. 5–17.

31. Bennett, K., and Embrechts, M., "An optimization perspective on kernel partial least squares regression," *Nato Science Series sub series III computer and systems sciences*, Vol. 190, 2003, pp. 227–250.

32. Rosipal, R., and Trejo, L. J., "Kernel partial least squares regression in reproducing kernel hilbert space," *Journal of machine learning research*, Vol. 2, (Dec), 2001, pp. 97–123.

33. Goodfellow, I., Bengio, Y., and Courville, A., *Deep learning*, MIT press, 2016.